Adiabatic creation of coherent superposition states in atomic beams

R. G. Unanyan,* M. E. Pietrzyk, B. W. Shore,† and K. Bergmann
Fachbereich Physik der Universität Kaiserslautern, 67653, Kaiserslautern, Germany
(Received 3 May 2004; published 11 November 2004)

We describe a technique for creating superpositions of degenerate quantum states, such as are needed for beam splitters used in matter-wave optics, by manipulating the timing of three orthogonally polarized laser beams through which moving atoms (or molecules) pass; motion across the laser beams produces pulses in the atomic rest frame. As illustrated with representative simulations for transitions in metastable neon, a single pass through three overlapping laser beams can produce superpositions (with preselected phase) of atomic beams differing by transverse momentum corresponding to the momentum of four photons. Like the two-photon momentum transfer of the tripod linkage pattern which it extends, the method relies on controlled adiabatic time evolution in the Hilbert subspace of two degenerate dark states. It is thus a generalization to multiple dark states (and larger transfers of linear momentum to the atomic beam) of the single dark state occurring with the stimulated Raman adiabatic passage (STIRAP) technique, and therefore it is potentially insensitive to decoherence due to spontaneous emission. By extending the tripod-linkage system to more numerous degenerate states, the technique not only increases the atomic beam deflections but, as we demonstrate, allows control over the superposition phase and amplitudes. LIke other techniques based on adiabatic time evolution, the technique is robust with respect to variations of the intensity, timing, and other characteristics of the laser fields. Unlike STIRAP, the same robust partial population transfer occurs for opposite timings of the pulse sequence, as is needed for such procedures as Hadamard gates.

DOI: 10.1103/PhysRevA.70.053404 PACS number(s): 42.50.Hz, 03.65.Ta

I. INTRODUCTION

A. Statement of the problem

There exist many techniques for transferring population completely and selectively from one quantum state—say, ψ_a—to another quantum state—say, ψ_b. Many of these techniques also provide the possibility to create a superposition of the two states—say, $\Phi(\theta)=\cos\theta\psi_a+\sin\theta\psi_b$ or, more generally,

$$\Phi(\theta,\varphi)=\cos\theta\psi_a+\exp(i\varphi)\sin\theta\psi_b, \tag{1}$$

with prescribe mixing angle θ and superposition phase φ.

When the two quantum states refer to internal excitation that accompanies the absorption of a photon (or, more generally, n photons) in an atomic or molecular beam experiment, then each transition necessarily accompanies a change of transverse momentum of the atom or molecule. In an n-photon transition the atom will absorb momentum $n\hbar k$ transverse to the atomic beam axis, where $k=\omega/c$ for a photon of angular frequency ω, and will undergo a corresponding deflection. The deflection may take place in two steps: absorption of forward-moving photons followed by stimulated emission of backward-moving photons—a total of n all together. The state superposition then corresponds to the creation of a coherent superposition of two matter waves having different momentum directions. Such superpositions of transverse center-of-mass motion are a key ingredient in schemes for creating matter-wave beam splitters, an essential element in the construction of an interferometer using matter waves rather than optical waves. Figure 1 illustrates schematically the momenta arrangements of such a superposition, in which each of the two beams is deflected by the angle $\phi=\arctan(nk/K_0)$ [1–5].

In principle, it is a simple matter to create such a superposition $\Phi(\theta,\varphi)$ using a resonant one-photon transition between nondegenerate states or, alternatively, a resonant two-photon Raman transition; the mixing angle θ is then just the temporal pulse area a:

$$\theta=a\equiv\int_{-\infty}^{\infty}dt\Omega(t), \tag{2}$$

basically the product of a peak Rabi frequency $\Omega(0)$ and the pulse temporal width T. To produce the desired 50:50 superposition it is only necessary to adjust the pulse area to be $\pi/4$. Such techniques obviously require careful control of

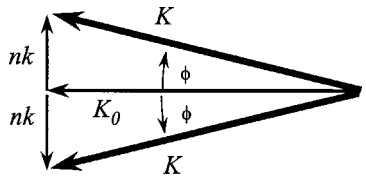

FIG. 1. Schematic diagram of superposition of beam deflection states, showing original (longitudinal) momentum K_0 of atoms, transverse momentum nk of the n-photon transition, and resulting atomic momentum K (all in units of $\hbar$). The resulting deflection is by angle $\phi=\arctan(nk/K_0)$.

*Permanent address: Institute for Physical Research, Armenian National Academy of Sciences, 328410 Ashtarak, Armenia.

†Permanent address: 618 Escondido Cir., Livermore, CA 94550, USA.

 ©2004 The American Physical Society

pulse areas, and hence they are sensitive to variations of both the peak intensity (i.e., the square of the Rabi frequency) and the pulse duration T.

A highly desirable property for any such technique is insensitivity to various characteristics of the pulses that produce the excitation. Such things as laser phase or pulse duration and intensity (pulse area), for example, may be difficult to control precisely. Adiabatic processes typically are more robust than techniques that rely on precisely controlled temporal pulse areas (as with so-called π pulses, whose temporal area is an odd-integer multiple of π). For π pulses the population change is often directly proportional to temporal area; under such a situation an error of 1% in pulse area will produce a 1% error in mixing angle. By contrast, adiabatic processes are insensitive to pulse area and can be made to depend only quadratically upon the principal experimental parameters, the temporal delay between pulses.

B. Historical context

One of the techniques frequently used for robust population transfer, and potentially available for the creation of superpositions, is stimulated Raman adiabatic passage (STIRAP) [6]. This technique uses two pulses, offset from each other in time, and the Raman coupling $\psi_a \leftrightarrow \psi_c \leftrightarrow \psi_b$. One of the conditions for successful complete population transfer $\psi_a \rightarrow \psi_b$ is that the two pulses occur with a definite time ordering (the so-called counterintuitive sequence) in which the *c-b* pulse precedes the *a-c* pulse. Such a pulse sequence is unsatisfactory for the return transition $\psi_b \rightarrow \psi_a$, and so STIRAP is not a technique available for constructing Hadamard transformations.

The addition of one more linked quantum state, extending the system from a three-state λ linkage to a four-state tripod linkage, provides the needed additional flexibility to devise pulse sequences that have prescribed effects on each of the potential starting (ground) states ψ_a or ψ_b [5,7,8].

The use of the STIRAP technique to produce deflection of an atomic beam as part of a beam splitter was first proposed by Marte *et al.* [1] and was subsequently demonstrated in beams of metastable helium [2] and cesium [3]. This concept was also demonstrated in a beam of metastable neon atoms, where two applications of a five-state STIRAP-like process led to beam momentum splittings of $8\hbar k$ [4]. Recently a four-state linkage in metastable neon, used with a STIRAP-like procedure, has been used to create a superposition of two states with arbitrary preselected phase, starting from a third state [9]. By contrast, the superpositions described in the present paper are of the initial state and a second state.

The STIRAP procedure makes use of a so-called *dark* state: an adiabatic state constructed from two stable or metastable states that do not fluoresce. The extension of the original three-state chain of STIRAP to longer chains, all with a single dark state, was discussed several years ago [10,11]. The benefits of extending the coherent dynamics of the single dark state of the λ system (or its generalizations) to the two dark states of the tripod system have been pointed out [7,8]. The experimental demonstration of superposition creation, and consequent beam splitting, in a tripod system was first demonstrated by Theuer *et al.* in a beam of metastable neon atoms [5]. The tripod system was subsequently proposed as the basis for a Hadamard gate by Duan *et al.* [12]. We note that linkage patterns allowing more than two dark states have been discussed, [13–15] although their use has not yet been exploited.

In the present paper we extend the previous work on tripod systems [5,8] to consider a generalization to larger numbers of coupled quantum states and two dark states, as occurs when one has transitions between degenerate angular momentum states. We will illustrate the proposal with simulations appropriate to metastable neon.

II. HAMILTONIAN

We consider a degenerate two-level system, having ground energies E_g and excited energies $E_e > E_g$, whose degeneracy originates in the orientation degeneracy of the angular momentum, J_g and J_e, of the ground and excited levels, respectively. We take the interaction to be that of an electric dipole $\mathbf{d}$ with the electric field $\mathbf{E}(t)$ evaluated at the center of mass of an atom moving with constant velocity v across laser beams. For an electric field expressible as a sum of polarization components in spherical coordinates, all at the same frequency $\omega = 2\pi c/\lambda$,

$$\mathbf{E}(t) = \sum_q \mathcal{E}_q(t)\mathbf{e}_q \cos(\omega t), \tag{3}$$

the electric dipole interaction Hamiltonian is

$$H^{int}(t) = -\mathbf{d}\cdot\mathbf{E}(t) = -\cos(\omega t)\sum_q (-1)^q d_q \mathcal{E}_{-q}(t). \tag{4}$$

Here $\mathcal{E}_{-q}(t)$ is the electric field amplitude (generally complex valued) associated with the unit polarization vector $\mathbf{e}_q$ and the dipole component d_q, for the three choices $q = -1, 0, +1$.

We make the usual rotating-wave approximation (RWA) by writing the state vector as

$$\Psi(t) = \exp[-i\zeta_g(t)]\sum_{M_g} C_{J_g M_g}(t)|J_g M_g\rangle + \exp[-i\zeta_e(t)]\sum_{M_e} C_{J_e M_e}(t)|J_e M_e\rangle \tag{5}$$

and choosing $\zeta_e(t) = \zeta_g(t) + \omega t$. In the Hamiltonian we replace the cosine with its cycle average $1/2$. With allowance for three independent polarization fields the interaction Hamiltonian matrix elements can be written, in the RWA, as

$$\langle J_e M_e|H^{RWA}(t)|J_g M_g\rangle = \frac{1}{2}(-1)^q \mathcal{E}_{-q}(t)\langle J_e M_e|d_q|J_g M_g\rangle. \tag{6}$$

Here and henceforth q is constrained to take the value $q = M_e - M_g$. We extract the dependence on magnetic quantum numbers as a Clebsch-Gordon coefficient using the Wigner-Ekart theorem (cf. [16], Sec. 20.5), writing

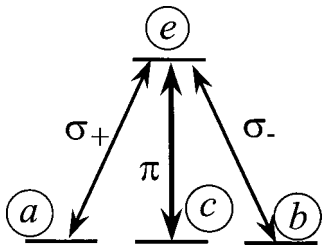

FIG. 2. Excitation between $J_g=1$ and $J_e=0$, showing separate links of σ_+, σ_-, and π polarization fields. Thick lines mark the two states between which a superposition is created.

$$\langle J_e M_e|H^{RWA}(t)|J_g M_g\rangle = -\frac{\hbar}{2}\Omega_q(t)(-1)^q\frac{(J_g M_g, 1q|J_e M_e)}{\sqrt{2J_g+1}},$$

where the Rabi frequency $\Omega_q(t)$ is proportional to the reduced dipole-moment matrix element $(J_e\|d\|J_g)\equiv d_{eg}$ and to the field amplitude $\mathcal{E}_q(t)$:

$$\hbar\Omega_q(t)\equiv\mathcal{E}_q(t)d_{eg}. \tag{7}$$

Although the Clebsch-Gordon coefficients are real values, as will be noted the field amplitudes may be complex valued, and so the Rabi frequencies also must be allowed this genrality.

A. Two-state superposition

Our concern is primarily the creation of a 50:50 superposition $(\theta=\pi/4)$ of two of the ground-state sublevels—namely,

$$|a\rangle=|J_g,-J_g\rangle \text{ and } |b\rangle=|J_g,+J_g\rangle, \tag{8}$$

with the notation $|J,M\rangle$ for an angular momentum state. Various atomic and molecular systems can be found on which to demonstrate the concepts presented above, involving two dark states. Here we discuss first a generic tripod scheme $(J_g=1)$, revealing in simplest form the basic principles. Such a scheme involves a two-photon transition from state a to state b, and hence a transverse momentum transfer from field to atom of $2\hbar k$. We follow this with a proposal for using a transition of metastable neon, for which $J_g=2$ and which offers the possibility of $4\hbar k$ momentum transfer. We show that, despite having a multiplicity of c states in this case, it is still possible to create the desired superposition state.

B. Tripod linkage pattern

Figure 2 illustrates the general linkages of the well-known tripod configuration [7,8,12,19], starting from the three sublevels of $J_g=1$ and ending with the single sublevel of $J_e=0$. The π linkages are present at all time, whereas the σ linkages are pulsed, sequentially. The superposition of interest involves the states $\psi_a=|J_g,-J_g\rangle\equiv|1,-1\rangle$ and $\psi_b=|J_g,+J_g\rangle\equiv|1,+1\rangle$.

C. Needed linkages

To create the desired linkages, a multistate generalization of the tripod system, we require laser beams capable of exhibiting each of the three orthogonal polarizations appropriate to spherical coordinates, usually termed σ_+, σ_-, and π. The selection rules for electric dipole radiation, assumed here, allow three types of linkages between upper and lower levels, distinguished by the selection rules

$$q=+1,\ M_e=M_g+1\ (\sigma_+ \text{ polarization}),$$

$$q=-1,\ M_e=M_g-1\ (\sigma_- \text{ polarization}),$$

$$q=0,\ M_e=M_g\ (\pi \text{ polarization}).$$

We will consider situations in which all three of these fields are present simultaneously. Because the sublevels are degenerate, all three types of transitions can be resonantly excited, as we shall assume, by a single frequency field $\hbar\omega=E_g-E_e$. Then all diagonal elements of the RWA Hamiltonian vanish.

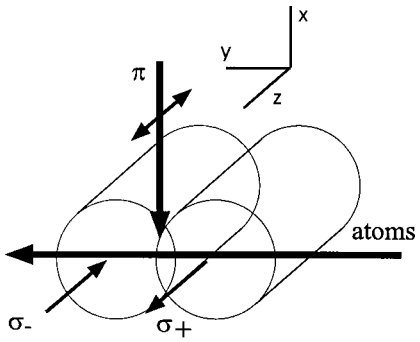

FIG. 3. Sketch of the propagation axes of the laser beams providing the σ_+, σ_-, and π polarization fields at the coordinate origin and of the atomic beam axis directed perpendicular to each of these.

Our interest here is with an atomic beam experiment (in contrast with experiments with trapped ions or atoms). We take the axis of the atomic beam to define the y axis. Then the first of these fields can be obtained from a circularly polarized laser beam propagating along the z axis, perpendicular to the atomic beam. By means of a beam splitter and mirrors, this same laser beam can serve as the source of the second field, propagating also along the z axis, possibly in the opposite direction. The third field, the π polarization, requires a laser beam propagating along the x axis, perpendicular to both of the σ beams and to the atomic beam, with linear polarization along the atomic beam axis. Figure 3 illustrates the assumed geometry of such situations, obtained from a single laser field, passing through a suitable arrangement of mirrors, lenses, beam splitters, and polarizers. The σ_+ and σ_- beams propagate in parallel, but spatially offset; the atomic beam travels perpendicular to each of these laser beams.

The result of these overlapping traveling-wave fields is seen, in a reference frame moving with the atomic center of mass, as a sequence of pulses. By suitably adjusting the beam widths and the separation of their centers, it is possible to create fields in the center of mass of the moving atoms as shown in Fig. 4: a long but weak π-polarization pulse that overlaps the two σ-polarization pulses. These latter pulses are offset from each other in time and will be assumed to have equal amplitudes. However, in addition to a temporal

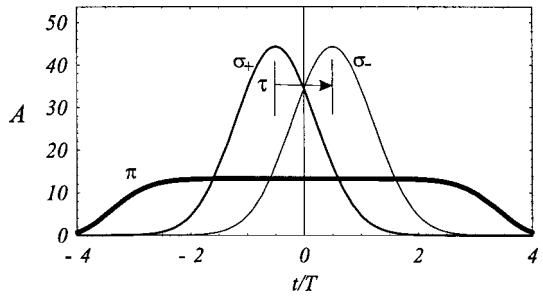

FIG. 4. Amplitudes A of σ_+, σ_-, and π polarization fields versus time t, as seen in the atomic reference frame. The σ_+ pulses precedes the σ_- by τ.

offset between the σ_+ and σ_- pulses, as seen by the moving atoms, there can be a phase delay $\Delta\phi$ between these two fields, perhaps originating in a different path length from the beam splitter; this appears as a phase of the field envelope $\mathcal{E}_q(t)$. As we shall demonstrate, phases do affect the excitation dynamics in this system.

D. Parametrizing the interaction

The time dependence of the pulsed field derives from the spatial variation of the laser beams, across which atoms move with constant speed v, and thus the temporal pulse shape is a direct transcription of the spatial beam profile. Although typical laser beams are idealized as Gaussians, advantages are to be expected from beam profiles whose central distribution has a slower variation. To demonstrate this we take the spatial profile to be of generalized Gaussian form. For those beams traveling along the z axis it is

$$E_q(x,y) = |\mathcal{E}_q(0)|\exp(-i\phi_q)\exp[-(x/vT)^n - (y/vT)^n], \quad (9)$$

and thus, with the assumption that the atoms pass through the beam center $(y=0, x=0)$, the time dependence is

$$\mathcal{E}_q(t) = |\mathcal{E}_q(0)|\exp(-i\phi_q)\exp[-(t/T)^n], \quad (10)$$

where the pulse duration T is obtainable, for given atom velocity v and beam waist w, as $T=w/v$. The power in the beam is evaluated as

$$p_q = \frac{c}{8\pi}\int_{-\infty}^{+\infty} dx \int_{-\infty}^{+\infty} dy |E_q(x,y)|^2 = \frac{c}{8\pi}|\mathcal{E}_q(0)|^2 \frac{(vT\mathcal{A})^2}{2}, \quad (11)$$

where $\mathcal{A}$ is the integral of the generalized Gaussian:

$$\mathcal{A} \equiv \int_{-\infty}^{+\infty} dx \exp[-x^n]. \quad (12)$$

Resonant two-state coherent excitation is often parametrized by the temporal pulse area, defined as the time integral of the Rabi frequency. When degeneracy is present, there are numerous dipole transition moments (from the numerous combinations of magnetic quantum numbers) and hence numerous Rabi frequencies. We shall use just three pulse areas a_q, $q=0,\pm1$, corresponding to the use of the single reduced dipole moment:

$$a_q = \frac{d_{eg}}{\hbar}\int_{-\infty}^{+\infty} dt \mathcal{E}_q(t) = \frac{d_{eg}}{\hbar}\mathcal{E}_q(0)T\mathcal{A}. \quad (13)$$

When expressed in terms of beam power p_q and atom velocity v as the two essential experimentally controllable parameters, the temporal pulse area a_q is independent of the beam waist:

$$a_q = \frac{d_{eg}}{\hbar v}\sqrt{\frac{8\pi p_q}{c}}. \quad (14)$$

Thus the peak Rabi frequencies are expressible variously as

$$|\Omega_q(0)| = \frac{d_{eg}}{\hbar}|\mathcal{E}_q(0)| = \frac{a_q}{\mathcal{A}} = \frac{d_{eg}}{\hbar w\mathcal{A}}\sqrt{\frac{8\pi p_q}{c}}. \quad (15)$$

E. Defining the pulses

We shall write the time dependence of the Rabi frequencies in terms of real-valued functions $f_q(t)$ having unit peak value

$$\Omega_q(t) = |\Omega_q(0)|f_q(t)\exp(-i\phi_q) \quad (16)$$

and explicit phases ϕ_q. To permit modeling a variation in the pulse shape we take the temporal shape to be a hyper-Gaussian (for $n=2$ this is a Gaussian)

$$f_{\pm1}(t) = \exp[-(t \pm 0.5\tau)^n/T^n], \quad (17)$$

$$f_0(t) = \exp[-(t/50T)^n]. \quad (18)$$

That is, the two σ polarization pulses are offset in time by τ and the π polarization pulse is essentially constant during the other pulses.

Although the magnetic sublevels associated with the lower-lying levels may remain immune to spontaneous emission loss, the upper sublevels have no such constraint. The assumed dipole linkages that produce laser-induced excitation will also provide links for spontaneous emission. The effect of such transitions can only be treated correctly by means of a density matrix equation; see the Appendix.

We are interested in partial population transfer between two of the degenerate magnetic sublevels of the lower-energy level. Specifically, we consider partial transfer between the two extremes, those with $M_g=-J_g$ and $M_g=+J_g$.

III. DARK STATES

As in previous work on the λ and tripod linkages, our interest lies with systems for which the degeneracy of the ground levels exceeds that of the excited level, so that at least one dark state exists. In particular, we assume that the angular momentum of the higher-energy level, J_e, is J_g-1. The total number of magnetic sublevels—and thus the total number of quantum states—is $N=4J_g$. The structure of the linkage patterns of interest, in which there exist two more quantum states of the lower degenerate level than of the upper degenerate level, means that for any combination of polarization linkages the system is equivalent, at any instant of

time, to a set of $N_b=2J_e+1=2J_g-1$ independent two-state systems (an excited state paired with a bright ground state), plus two additional states (dark states) constructed from the set of ground states [17]. These have no connection to the excited states; they are unaffected by the radiation at that moment. The composition of these two dark states varies as the pulse polarizations vary, but they never include any component from the upper manifold of states. Thus the dark states never undergo spontaneous emission—they do not fluoresce.

This property, of multiple dark states, differs from the situation in STIRAP, where there is only a single dark state. In that case it is possible to transfer population from state ψ_a to state ψ_b via counterintuitive pulses (Stokes before pump) or to create a superposition of these states starting from state ψ_a, but the requirement of counterintuitive pulses means that these pulses will not transfer population from ψ_b back to ψ_a; nor will they create a desired superposition starting from state ψ_b: there is an asymmetry between the states of this system which prevents the use of STIRAP for the creation of a Hadamard gate, for example.

The situations discussed in the present paper also differ from the tripod linkage discussed earlier in having more than one state comprising what is here termed the c set—degenerate ground states that are neither the a state or the b state. As will be demonstrated, the extra complication does not prevent a similar production of a superposition; in fact, it allows control of the phase of this superposition

In treating adiabatic evolution it is desirable to use the adiabatic states $\Phi_j(t)$, solutions to the eigenvalue equations

$$H(t)\Phi_j(t)=\varepsilon_j(t)\Phi_j(t). \tag{19}$$

The adiabatic states are orthogonal and are assumed normalized, $\langle\Phi_i(t)|\Phi_j(t)\rangle=\delta_{ij}$. We know that in our system there exists a subspace of two degenerate dark states, which we take to be the first two of this set. They are identifiable by their null eigenvalues, $\varepsilon_1(t)=\varepsilon_2(t)=0$.

We aim to start in a state within this two-dimensional dark space and to ensure that the time evolution thereafter is adiabatic, as will happen if the energy separation between the adiabatic energies of the dark states and those of any other adiabatic state is large. Under these conditions we can write the state vector as

$$\Psi(t)=A_1(t)\Phi_1(t)+A_2(t)\Phi_2(t). \tag{20}$$

Such a restriction to the subspace of two dark states is justified if the initial state is within this subspace (as it will be in our systems) and if the subsequent evolution is adiabatic. The condition for this can be shown to be that all the pulse areas be large:

$$\Omega_q T\gg 1,\ q=0,\pm 1. \tag{21}$$

Because these two adiabatic states are degenerate, their amplitudes $A_j(t)$ will not remain constant. Their changes are governed by the equations

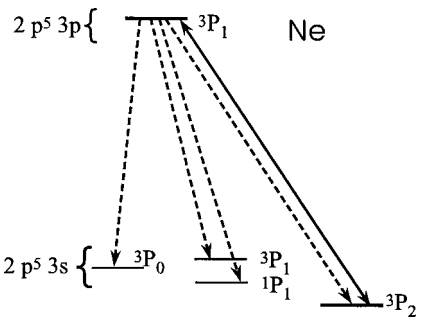

FIG. 5. Energy levels and transitions in metastable neon. The transitions of interest (shown by heavy line) are at wavelength 0.588 μm, between magnetic sublevels of $^3P_2$ and $^3P_1$. Dashed lines show spontaneous emission paths.

$$\frac{d}{dt}A_1(t)=-V(t)A_2(t),\ \frac{d}{dt}A_2(t)=-V(t)A_1(t), \tag{22}$$

where the coupling is

$$V(t)=\left\langle\Phi_1(t)\left|\frac{d}{dt}\Phi_2(t)\right.\right\rangle. \tag{23}$$

It follows from Eq. (22) that after the conclusion of all pulsed interaction, which we take to be as $t\to\infty$, the adiabatic amplitudes take the values

$$A_1(+\infty)=A_1(-\infty)\cos(\gamma)-A_2(-\infty)\sin(\gamma), \tag{24}$$

$$A_2(+\infty)=A_1(-\infty)\sin(\gamma)+A_2(-\infty)\cos(\gamma), \tag{25}$$

where the dark-state mixing angle is the integral of the coupling:

$$\gamma=\int_{-\infty}^{+\infty}dtV(t). \tag{26}$$

Unlike the mixing angle of single-photon excitation, this angle does not depend on the pulse area: it is a *geometrical* rather than *dynamical* angle [8,12,18,19].

A. Linkage pattern of neon

Figure 5 shows the important transitions of metastable neon. The two degenerate levels considered are $^3P_1(J_e=1,M_e=-1,0,1)$ and $^3P_2(J_g=2,M_g=-2,\ldots,2)$. The superposition of interest involves the states $\psi_a=|J_g,-J_g\rangle\equiv|2,-2\rangle$ and $\psi_b=|J_g,+J_g\rangle\equiv|2,+2\rangle$. The complete transfer of population corresponds to a transverse momentum change from four photons. We denote the corresponding probabilities, following pulse completion, as P_a and P_b.

Spontaneous emission occurs from the $^3P_1$ levels to the lower-lying $^3P_1$ and $^1P_1$ levels of the $2p^53s$ configuration, with rates, respectively, $\gamma_{decoh}=0.011\ \mathrm{ns}^{-1}$ and $\gamma_{out}=0.0438\ \mathrm{ns}^{-1}$. Of these decays, 20% goes to the $^3P_2$ level of interest.

Figure 6 illustrates the general linkages of this situation. The π linkages are present at all time, whereas the σ linkages are pulsed, sequentially. The Appendix presents the RWA Hamiltonian matrix elements in detail.

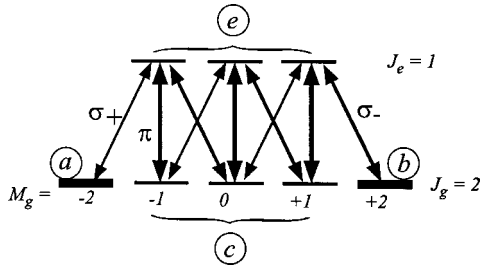

FIG. 6. Excitation between $J_g=2$ and $J_e=1$, showing separate links of σ_+, σ_-, and π polarization fields. Thick horizontal lines mark the two states between which a superposition is created.

As with the tripod system, there are two dark states for this system. However, the transition between states a and b involves four photons, so this transfer will be accompanied by a linear momentum change of $4\hbar k$.

B. Useful observables

To complete the definition of the superposition states we require the angle φ of Eq. (1). Our goal can be usefully quantified through the use of a two-state density matrix by defining the populations $P_a(t) \equiv \rho_{aa}(t)$ and $P_b(t) \equiv \rho_{bb}(t)$ together with the Bloch variables

$$u(t) + iv(t) = \rho_{ab}(t) \text{ and } w(t) = \rho_{bb}(t) - \rho_{aa}(t) \qquad (27)$$

for the two states of interest. A typical objective is to start all the atoms in state a, with initial conditions $u(t)=v(t)=0$ and $w(t)=-1$ at $t \to -\infty$, and by subjecting the atoms to a crafted pulse sequence to obtain the results $|u(t)|=1$ and $v(t)=w(t)=0$ after the pulse completion, at $t \to +\infty$. The goal of creating a 50:50 superposition corresponds to rotating the Bloch vector by $\pi/2$ from its initial alignment.

IV. SIMULATION RESULTS

In this section we provide illustrative simulations of pulsed excitation of the two systms defined in the previous section: a simple four-state tripod system and a more elaborate eight-state linkage system.

A. Essential parameters

We shall assume that the two σ-polarization pulses have the same peak intensities, meaning that areas $a_{+1}=a_{-1} \equiv a$, and have the same pulse widths T, but we allow them to have different phases; they are offset in time by τ. When solving the Schrödinger equation it proves useful to express all times in multiples of the pulse duration T (accomplished by setting $T=1$ in the various algebraic expressions) and to express the three-peak Rabi frequencies $\Omega_q(0)$ in terms of pulse area and phase, $\Omega_q(0)=a_q/\mathcal{A}\exp(i\phi_q)$, where $\mathcal{A}$ is the normalization area of Eq. (12).

We assume that the π-polarization pulse is of much longer duration than these pulses and that its peak value is centered midway between the other two pulses. For computations we often take it to be of constant amplitude. We characterize this field by the ratio of peak electric field amplitudes or, what is the same thing,

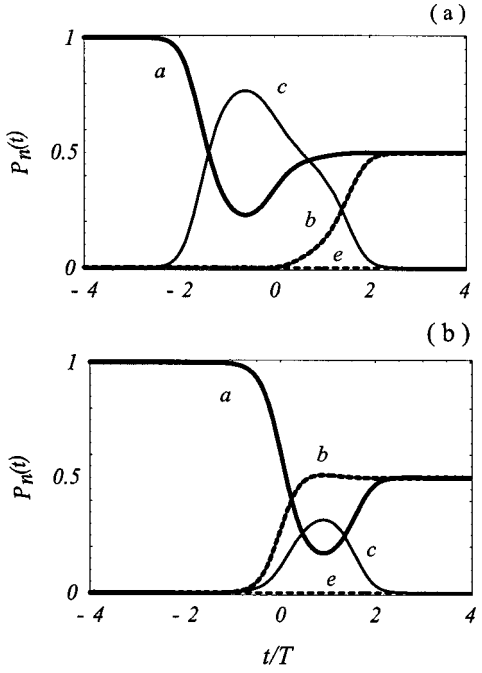

FIG. 7. Time dependence of populations in the initial state (a), the target state (b), and the intermediate state (c) for the tripod system. (a) Pulses in intuitive order (σ_+ precedes σ_-, $\tau=+1.2$). (b) Pulses in counterintuitive order (σ_- precedes σ_+, $\tau=-1.2$). Parameters: $a=50\pi$, $\tau=1.2$, and $\beta=0.54$. Phases: $\phi_{-1}=0$, $\phi_0=0$, and $\phi_{+1}=\pi$.

$$|\Omega_0(0)| = \beta|\Omega_{+1}(0)| = \beta|\Omega_{-1}(0)|. \qquad (28)$$

The excitation dynamics is affected also by the phase of this field, as we note in Sec. IV F.

Even with the foregoing simplifications, several parameters are needed to describe the pulse sequence: one pulse area a, the ratio of amplitudes β, the delay τ, and, taking the phase of the σ_- pulse as a reference, the two phases ϕ_{+1} and ϕ_0. As befits adiabatic procedures, there is typically a minimum value of the area a that must be exceeded for the results to be satisfactory, but any larger area will produce the same results. As will be noted, there are particularly desirable choices for the two adjustable phases. Thus the search for optimum conditions for producing a specified superposition [and a corresponding optimum path in the parameter space $(\Omega_+, \Omega_0, \Omega_-)$] reduces essentially to a search in a two-dimensional parameter space, that of β and τ.

B. Tripod system

The dynamics of the tripod system has been considered earlier in some detail [7,8,12,19]. As has been noted, it is possible to achieve population balance using pulses ordered either intuitively (the σ_+, connected with the initially populated state a, occurs first) or counterintuitively (the σ_- occurs first). The two orderings correspond to atoms passing through the laser beams in opposite directions. Figure 7 illustrates these two possibilities. The plots display the time

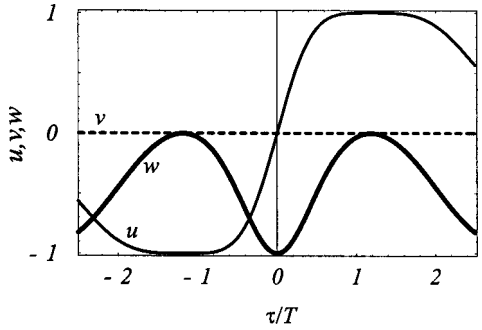

FIG. 8. Bloch variables u, v, and w for the tripod system at the end of the pulse sequence, as a function of delay τ. Parameters: $a=50\pi$ and $\beta=0.54$. Phases: $\phi_{-1}=0$, $\phi_0=0$, and $\phi_{+1}=\pi$.

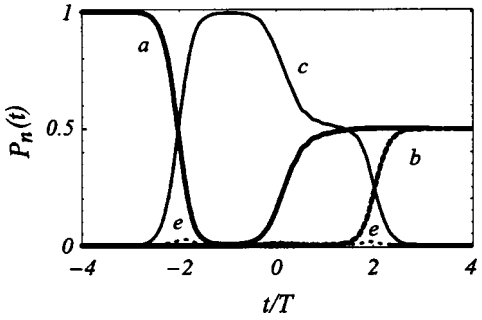

FIG. 9. Time dependence of populations in the initial state (a), the target state (b), and all other ground states (c) for the neon system. Parameters: $a=200\pi$, $\tau=1.5$, and $\beta=0.318$. Phases: $\phi_{-1}=0$, $\phi_0=0$, and $\phi_{+1}=\pi$.

dependence of the populations in the states of interest, a, b, and c. This latter population is only transient: at the end of the pulse sequence only states a and b have population. The population in the excited state e is at all times too small to be seen.

Some idea of the adiabatic nature of the evolution displayed in Fig. 7 can be obtained from the time-integrated population in the excited state, $\int dt P_e(t)$. For Fig. 7(a) this value is $1.4\times10^{-3}T$, while for Fig. 7(b) it is $7\times10^{-4}T$.

In obtaining these plots, which demonstrate successful 50:50 superposition but without indication of the phase, we first fixed the pulse area and phases, and then iteratively found satisfactory values for τ and β.

To appreciate the complementarity of these two delay values and to see the phase of the superposition, it is useful to examine values of the Bloch variables at the end of the pulse sequence. For a perfect 50:50 superposition (maximal coherence) these values are $w=0$ and $u^2+v^2=1$. Figure 8 shows such a plot. The equality of population ($w=0$) occurs here at $\tau=\pm\tau_e$, where $\tau_e=1.2T$. We see that the population inversion w is symmetric about $\tau=0$, but that the curve of the phase-sensitive variable u vs τ is antisymmetric; when $\tau=+\tau_e$, we find $u=+1$, while for $\tau=-\tau_e$ the coherence is $u=-1$. These two values are associated with the two coherent superpositions $|a\rangle\pm|b\rangle$. It should be noted that these simple symmetry properties occur only when the evolution is adiabatic.

C. Metastable neon: Numerical values

Although the simulation of this system need make no specific reference to either the laser power or the the laser intensity, it is useful to associate various choices of pulse area with realistic values of those quantities. For that purpose it is only necessary to have available a dipole moment. To obtain the reduced dipole transition moment d_{eg} we use the connection between the Einstein A coefficient (here in cgs and then atomic units):

$$A_{eg}=\frac{4}{3\hbar}\left(\frac{\omega}{c}\right)^2\frac{|d|^2}{g_e}=\frac{1}{\tau_{\text{a.u.}}}\frac{4}{3}\left(\frac{2\pi a_0}{\lambda}\right)^2\frac{S_{eg}}{g_e} \tag{29}$$

and the transition strength

$$S_{eg}=S_{ge}\equiv|d_{eg}|^2\equiv\frac{(J_e\|d\|J_g)^2}{ea_0}{}^2. \tag{30}$$

We then have the formula

$$d_{eg}\equiv\frac{(J_e\|d\|J_g)}{ea_0}\equiv\sqrt{S_{eg}}=\sqrt{(2J_e+1)\tau_{\text{a.u.}}A_{eg}\frac{3}{4}\frac{\lambda^3}{(2\pi a_0)^2}}$$
$$=22.216\sqrt{(2J_e+1)A_{eg}[\text{ns}^{-1}](\lambda[\mu\text{m}])^3}. \tag{31}$$

For neon, using the value $A_{eg}=1.1\ \text{ns}^{-1}$ for $\lambda=533\ \mu$m, we obtain a dipole moment $d_{eg}=1.819\,66$. With this dipole moment and a representative velocity $v=10^3$ m/s, a pulse area of 200 π corresponds to beam power of 12.2 mW. With a beam waist of 2 mm, the peak intensity is 0.19 W/cm^2, the pulse duration is $T=2000$ ns, and the peak Rabi frequency is 0.18 rad/ns.

D. Gaussian beams: Optimizing β and τ

In the following sections and figures we consider the extension of the four-state tripod results shown above to the eight-state neon system. We first consider purely Gaussian beams, $n=2$ in Eq. (17). With a suitable choice of area, phases, delay, and β one finds a time dependence as shown in Fig. 9. Here, as in Fig. 7, are displayed the time dependence of the populations in the states of interest, a and b, but now c denotes the summed populations in all the other three ground states. This latter population is only transient: at the end of the pulse sequence only states a and b have population. The population in the excited states is at all times too small to be seen; the time integral of $P_e(t)$ is $1.6\times10^{-3}T$.

Figure 9, appropriate to neon, is to be compared with frame (a) of Fig. 7, for the tripod system. The qualitative behaviors of curves a and c are similar, but they are by no means identical.

In obtaining this plot, which demonstrates successful 50:50 superposition but without any indication of the phase, we first fixed the pulse area and phases, and then iteratively found satisfactory values for τ and β. A similar superposition, but with opposite phase, is obtained with the choice $\tau=-1.5$ while all other parameters remain the same. This solution corresponds to a situation where the atoms move across the beams in the opposite directions. Figure 10 shows

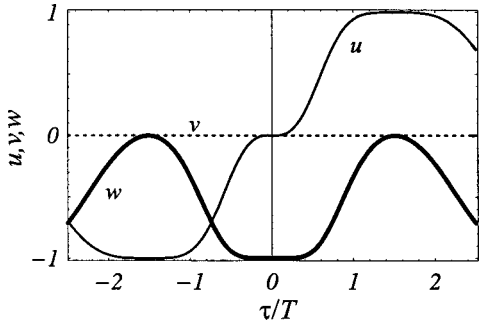

FIG. 10. Bloch variables u, v, and w at the end of the pulse sequence, as a function of delay τ. Parameters: $a=200\pi$ and $\beta=0.318$. Phases: $\phi_{-1}=0$, $\phi_0=0$, and $\phi_{+1}=\pi$.

such a plot. The equality of population ($w=0$) occurs here at $\tau=\pm\tau_e$, where $\tau_e=1.2T$. We see that the population inversion w is symmetric about $\tau=0$, but that the curve of the phase-sensitive variable u vs τ is antisymmetric; when $\tau=+\tau_e$, we find $u=+1$, while for $\tau=-\tau_e$ the coherence is $u=-1$. These two values are associated with the two coherent superpositions $|a\rangle\pm|b\rangle$.

Figure 10 displays results for an optimal choice of the Rabi ratio—namely, $\beta=0.318$. This plot is qualitatively similar to Fig. 8. In both cases the curve of w vs τ is symmetric about $\tau=0$ and that of u vs τ is antisymmetric. However, the details of the two plots differ noticeably.

In making these plots we selected β so that w approached but did not exceed 0. Figure 11 illustrates the effect of varying the choice of β. When β is larger than the optimum value, the inversion w is never complete for any delay. When

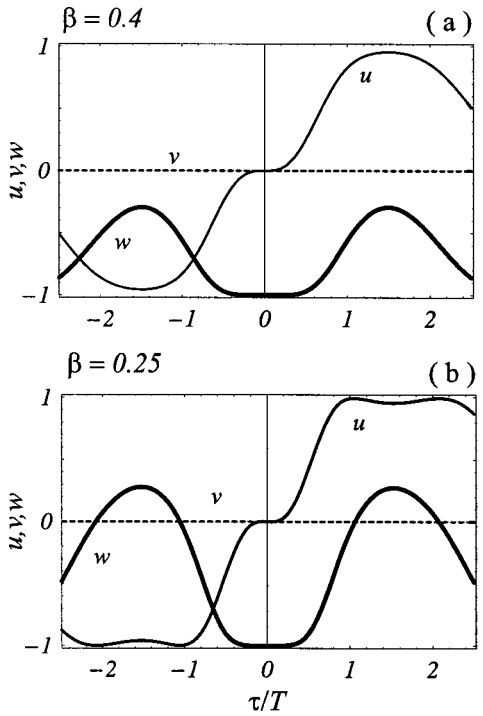

FIG. 11. Bloch variables u, v, and w at the end of the pulse sequence, as a function of delay τ. Parameters are area$=200\pi$ and (a) $\beta=0.4$ and (b) $\beta=0.25$.

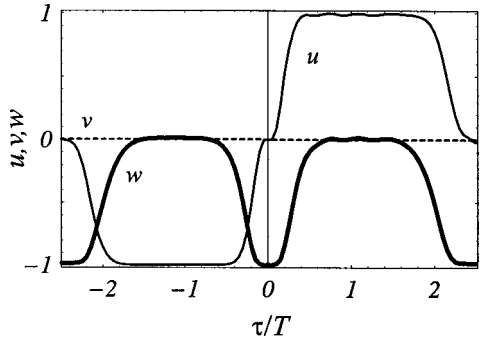

FIG. 12. Bloch variables u, v, and w at the end of the pulse sequence, as a function of the delay τ, for a Gauss-6 beam [$n=6$ in Eq. (10)]. Parameters are: area$=400\pi$ and $\beta=0.363$.

β is smaller than optimum, there are four possible values for which $w=0$ and 50:50 superpositions occur. However, unlike the situation of Fig. 10, where an error in choice of τ affects the superposition quadratically, here the effect of such an error is linear, and therefore these choices of β are less desirable.

E. Effects of the pulse shape: Hyper-Gaussian beams

Gaussian profiles are the usual forms assumed for focused laser beams, but in principle other shapes are possible. As the beams become more rectangular, there is a longer interval of delay over which the 50:50 superposition occurs. Figure 12, for a Gauss-6 beam [$n=6$ in Eq. (9)], illustrates this.

The increasing rectangularity of the pulse does not prevent adiabatic evolution and has definite advantages: the production of population equality is less sensitive to the choice of pulse delay. With increasing n there occurs an increasingly wide range of delay values for which the desired superposition occurs.

F. Effects of the pulse phase

For the tripod system the relative phases of the pulses only affects the phase of the superposition (i.e., whether u or v or some combination occurs when $w=0$). However, for $J_g=2$ the relative phase of the two σ pulses has a profound effect on the excitation dynamics. This can be seen even in the simple choice of a change in sign, as is obtained with the choice $\phi_{-1}=\phi_{+1}=0$, rather than the choice above in which the two phases differed by π. Figure 13(a), for equal phases, illustrates this assertion. Here there are four possible choices for τ that will give the desired superposition. Figure 13(b) shows the τ dependence when the two σ are 90° out of phase. In this case a 50:50 superposition is possible at two times, but at each of these both u and v are nonzero: the superposition has a complex phase.

The phase of the π-polarization pulse also matters. Figure 14 shows the Bloch variables as a function of this phase. As can be seen only the choices $\phi_0=n\pi$ for integer n will allow the desired superposition.

G. Understanding the effect of the pulse phase

An understanding of the dynamics can be obtained by considering first a four-state tripod linkage, with population

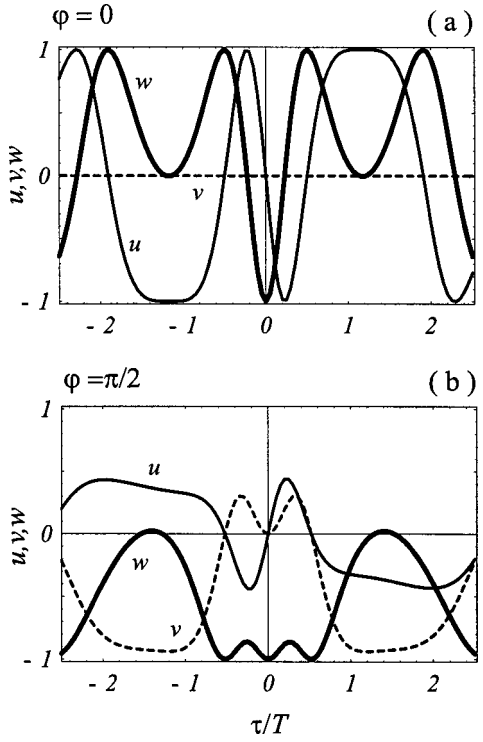

FIG. 13. Bloch variables u, v, and w at the end of the pulse sequence, as a function of delay τ. Parameters are area$=400\pi$, (a) $\phi_{+1}=0$, $\beta=0.493$, and (b) $\phi_{+1}=\pi/2$, $\beta=0.19$.

initially in state a, as indicated in Fig. 15(a). This system is to be subjected to a long π pulse and a sequence of σ_+ and σ_- pulses. We can regard the overall dynamics as three stages.

(i) In the initial stage, prior to the presence of the σ_- pulse, there is first a π pulse and then a stronger σ_+ pulse. These two provide the conventional counterintuitive pulse sequence (of STIRAP) to transfer all population from state a into state c, a temporary residence; see Fig. 15(a).

(ii) In the second stage of the interaction all pulses are present: the π and σ_+ pulses form an "intuitive" sequence for reversing the population transfer from state c back into state a. The σ_- pulse serves to produce a dynamic Stark shift of these two states, thereby preventing continued two-photon resonance. Therefore only a portion of the population returns

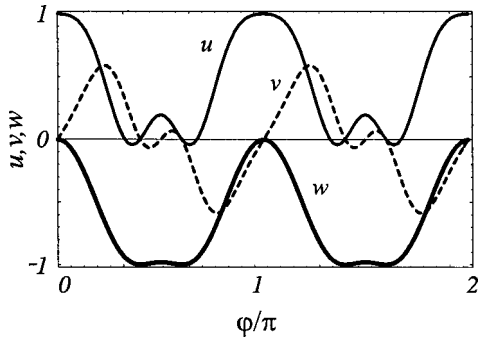

FIG. 14. Bloch variables u, v, and w at the end of the pulse sequence, as a function of the phase ϕ_0. Parameters are area $=400\pi$, $\tau=1.2$, and $\beta=0.318$.

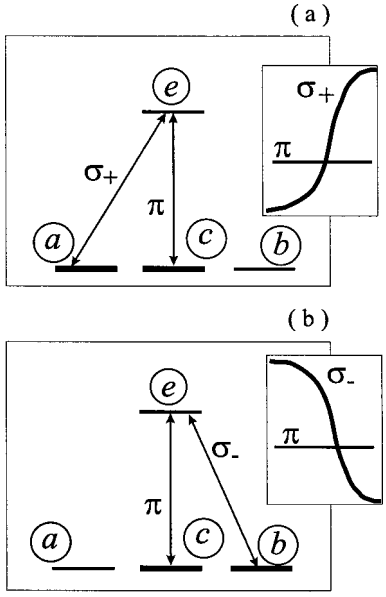

FIG. 15. Tripod-system linkage patterns (a) initially and (b) finally. Insets show schematic pulse forms appropriate to the linkage.

to state a, and a coherent superposition is created. The amplitudes of this superposition do not depend on the phases of the applied pulses.

(iii) In the final stage of the interaction only the σ_- and π pulses are present; see Fig. 15(b). These provide a counter-intuitive (STIRAP) sequence for moving population from state c into state b, the desired final destination. Because some population has returned during stage 2 into state a, the final result is a coherent superposition of states a and b.

The situation is more complicated when there are more linkages, as is the case with metastable neon we have considered above; see Fig. 16. Nevertheless, we can identify three stages of the dynamics.

(i) In the initial stage, prior to the presence of the σ_- pulse, there is first a π pulse and then a stronger σ_+ pulse. The resulting "counter-intuitive" pulse sequence transfers population into one of the c states; see Fig. 16(a).

(ii) In the second stage of the interaction all pulses are present. There is population transfer back into state a. During this stage the various state vector amplitudes acquire phases that depend on the phases of the laser pulses.

(iii) In the final stage of the interaction only the σ_- and π pulses are present; see Fig. 16(b). Population moves from the c states into state b. The phases of the c-state components is critical in determining the result of the final stage.

H. Decoherence processes

In an atomic beam experiment collisions have no influence, but the possibility of spontaneous emission is always present. Only this mechanism can produce changes not predicted within the coherent dynamics of the Schrödinger equation.

As described here, the successful creation of a superposition takes place by means of adiabatic time evolution in which the state vector is restrained to a degenerate dark

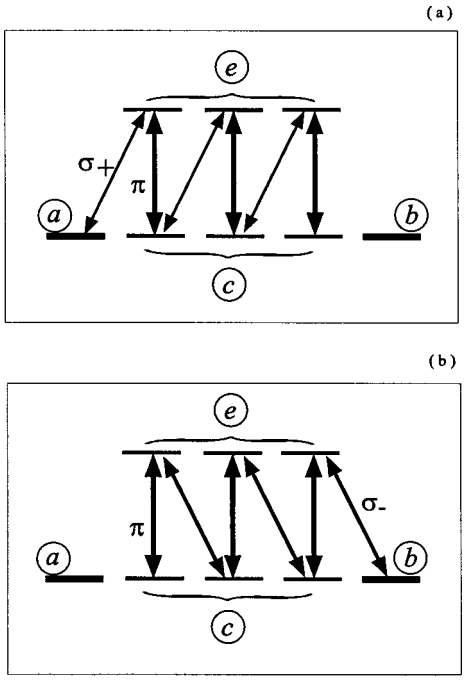

FIG. 16. *J* linkage patterns (a) initially and (b) finally.

space. Were the time evolution to be completely adiabatic, then no population would be present in the excited states at any time, and therefore spontaneous emission could not take place. Such time dependence can be successfully modeled using the Schrödinger equation. The dependence on such experimentally controlled quantities as beam power, beam waist, and atomic velocity occur only through the single parameter, the temporal pulse area (time integral of the Rabi frequency).

The time evolution in any real experiment will deviate to some extent from the adiabatic ideal, and with this deviation some population may come temporarily into the excited states. Thus it is desirable to verify that the assumed adiabatic evolution does describe situations of possible experimental interest.

We expect that when pulses are shorter than the spontaneous emission lifetime, meaning $\gamma T<1$, then any excited-state population will have little liklihood of decaying, and hence we expect the Schrödinger equation to remain satisfactory, even though the evolution may not be adiabatic. Only when the pulses become much longer can the effects of spontaneous emission be felt. But as the pulses become longer, we expect the evolution to become more adiabatic, and so the influence of the excited states should become less evident.

If spontaneous decay proceeds primarily to states other than those of the set of states being modeled by coherent excitation (i.e., the system is "open"), then such effects can be satisfactorily treated by simply including a loss (imaginary energy) from the upper state. However, with the neon system considered here this is not a good approximation: an appreciable fraction of the decays are to the states of interest. Such a situation requires treatment using a density matrix. The lifetime of the $^3P_1$ state of neon, 18 ns, provides the needed time scale for simulating the effects of spontaneous emission; the condition $\gamma T=1$ implies $T=18$ ns.

To verify the validity of our approximation, under assumed experimental conditions, we have carried out simulations using more elaborate density matrix equations of motion, as discussed in the Appendix. These are for the full set of eight sublevels, not just the *a*-*b* pair, and they take into account both the losses of probability from spontaneous emission outside of the chosen two degenerate levels, and the return of population within the chosen set.

With the density matrix equations the behavior can be considered as depending on two parameters: the pulse area (an absolute quantity) and the pulse duration relative to the lifetime of the excited state, or γT. For the simulations reported in previous sections we have taken the pulse area to be 200π. With this value the population in the excited state is seen to be small, and the results are seen to be essentially independent of pulse area. However, with the beam parameters mentioned above, including a pulse duration of $T=2000$ ns, we have $\gamma T>100$, and so even a small transient excitation can have an appreciable effect.

The error produced by spontaneous emission affects our results in two ways.

(i) Loss of probability out of the eight-state manifold will mean that fewer atoms remain in any superposition. Loss from the two-state manifold will similarly diminish the available atoms. To measure this effect we examine the normalization $\varepsilon_w=1-\mathrm{Tr}\rho$, where ρ is the 2×2 density matrix of the *a*-*b* sublevels.

(ii) Within this reduced numbers of atoms there will occur loss of coherence, as measured by the error $\varepsilon_u=u/\mathrm{Tr}\rho-u_{coh}$ between the Bloch component u in the presence of spontaneous emission and the value u_{coh} obtained by neglecting all spontaneous emission. Among those atoms that have not been lost to other manifolds, this is a measure of the attainable coherence and, hence, of the coherence loss due to spontaneous emission.

Figure 17 shows examples of the effect of spontaneous emission upon the two-state normalization, as a result of (a) varying the pulse duration (by adjusting the beam waist or the atomic velocity) or (b) as a result of varying the pulse area (by adjusting the beam power). The uppermost curves of the two frames are the same; the subsequent curves reveal how errors can be improved either by making the pulses shorter so that the atom spends less time in the excited state or by increasing the power, so that the evolution is more adiabatic.

As can be seen, even though the excited-state population is never large, the product of this population with γT can be appreciable. Thus considerable population is lost when one has pulses as long as 2000 ns.

It is significant that, although population is lost and therefore fewer atoms are available to provide the desired superposition nevertheless the superpositions of the remaining atoms remains good. Figure 18 shows examples of the effect of spontaneous emission upon the coherence, as a result of varying the pulse duration (by adjusting the beam waist or the atomic velocity) or as a result of varying the pulse area (by adjusting the beam power).

These plots show that the experimental conditions described earlier should suffice to permit the formation of co-

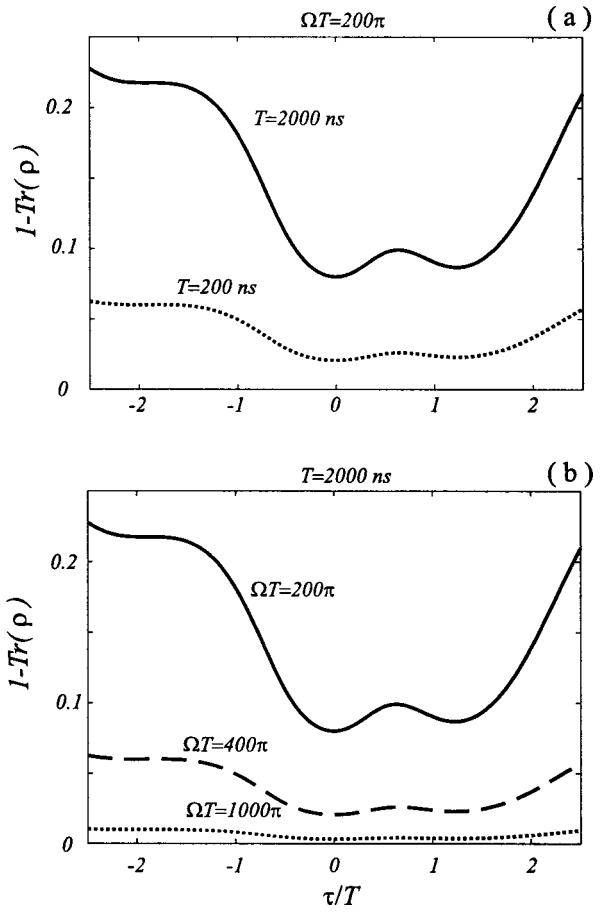

FIG. 17. Normalization error, $\varepsilon_w = 1 - \mathrm{Tr}\rho$ as a function of delay τ. (a) For fixed area 200π, varying the pulse duration T, 2000 ns and 200 ns. (b) For fixed $T = 2000$ ns, varying the pulse area, 200π, 400π, and 1000π.

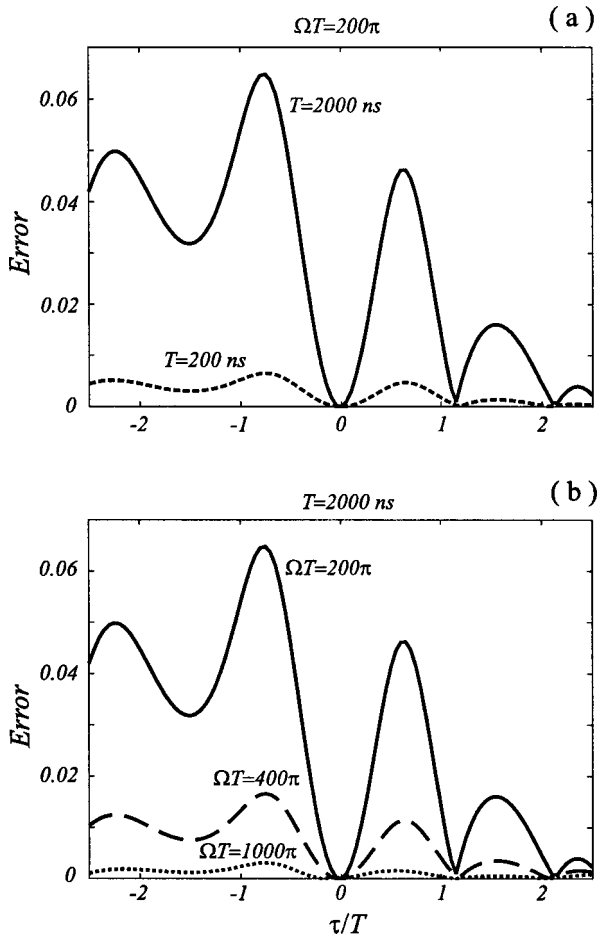

FIG. 18. Coherence error $\varepsilon_u = u/\mathrm{Tr}\rho - u_{coh}$ as a function of delay τ. (a) For fixed area 200π, varying the pulse duration T, 2000 ns and 200 ns. (b) For fixed $T = 2000$ ns, varying the pulse area, 200π, 400π, and 1000π.

herences with degradation error of around 0.04 and that an increase of power by a factor of 25 (a factor of 5 in Rabi frequency) would be needed to drop this error to 0.01.

V. SUMMARY AND CONCLUSIONS

In common with other coherent excitation schemes for manipulating atomic beams, our scheme requires a preliminary step of optical pumping to replace the typical thermal distribution of populations among all magnetic sublevels by a situation in which all atoms are in a single quantum state of internal excitation, termed here the a state. From this start, the three laser beams produce the desired superposition of internal excitation and the consequent superposition of the transverse translational motion.

We mention that this preparation can be done without loss of population by optical pumping with circularly polarized light on the $^3P_2$-$^3D_3$ transition, since this forms a closed system.

Our proposed scheme for producing 50:50 superpositions is an adiabatic process. As such, it can be improved by increasing the pulse areas of the σ pulses, with consequent increase in laser-power requirements. In particular, the contamination (and consequent decoherence from spontaneous emission) from excited states can be lessened by using larger pulse areas.

Extension from the tripod to more general linkage systems, associated with angular momentum larger than 1, is readily accomplished. The general principles acting to achieve coherent superpositions with the tripod system work equally well for more general systems; it is only necessary that $J_g > J_e$, so that there be two dark states. As the angular momentum increases, so too will the momentum transfer and, in turn, the separation of the two beams from a beam splitter. Thus it is advantageous to use large angular momenta.

The creation of a superposition state in the manner described in the present paper has a symmetry of initial and final states that is absent with conventional STIRAP: starting with either initial state and applying a fixed pulse sequence, one arrives through adiabatic evolution to a specific superposition—say, $|a\rangle + |b\rangle$. Subsequent reversal of the pulses returns the system to the initial state. This can be understood by following the evolution of the Bloch vector from pole to equator and back. Such behavior is needed for the construction not only of beam splitters and atomic optics elements, but also for the construction of Hadamard gates

and other elements needed for quantum information processing.

Our simulations with the density matrix give an idea of the degree to which the proposed superpositions can be accomplished in the presence of spontaneous emission. With known radiative properties of neon and assumed values of the lasers and atomic beam, errors of 0.04 or less should be possible; these can be reduced by increasing the laser power or shortening the pulse duration.

ACKNOWLEDGMENTS

We are grateful for suggestions from Michael Fleischhauer. R.G.U. acknowledges support from the Alexander von Humboldt Foundation and the Deutsche Forschungsgemeinschaft, under Contract No. Fl-210/10. M.E.P. acknowledges support from the European Union network Complex Quantum Systems (QUACS).

APPENDIX: SIMULATING SPONTANEOUS EMISSION

To test the the applicability of the Schrödinger equation to the neon system we used density matrix equations. We took these to be of Lindblad form [20]

$$\frac{\partial\rho}{\partial t} = -i[H^{RWA},\rho] - \frac{\gamma_{out}}{2}L\rho - \frac{\gamma_{out}}{2}\rho L + \frac{\gamma_{decoh}}{2} \times \sum_{\mu=-1}^{1}[L_\mu\rho, L_\mu^\dagger] + \frac{\gamma_{decoh}}{2}\sum_{\mu=-1}^{1}[L_\mu, \rho L_\mu^\dagger]. \quad \text{(A1)}$$

The coefficients γ_{decoh} and γ_{out} are, as defined in Sec. III A, $\gamma_{decoh}=0.011$ ns^{-1}, and $\gamma_{out}=0.0438$ ns^{-1}. The RWA Hamiltonian matrix H^{RWA} is $1/\sqrt{10}$ times:

$$\begin{bmatrix} 0 & 0 & 0 & \sqrt{6}\Omega_+ & \sqrt{3}\Omega_0 & -\Omega_- & 0 & 0 \\ 0 & 0 & 0 & 0 & \sqrt{3}\Omega_+ & 2\Omega_0 & -\sqrt{3}\Omega_- & 0 \\ 0 & 0 & 0 & 0 & 0 & \Omega_+ & \sqrt{3}\Omega_0 & -\sqrt{6}\Omega_- \\ \sqrt{6}\Omega_+ & 0 & 0 & 0 & 0 & 0 & 0 & 0 \\ \sqrt{3}\Omega_0 & \sqrt{3}\Omega_+ & 0 & 0 & 0 & 0 & 0 & 0 \\ -\Omega_- & 2\Omega_0 & \Omega_+ & 0 & 0 & 0 & 0 & 0 \\ 0 & -\sqrt{3}\Omega_- & \sqrt{3}\Omega_0 & 0 & 0 & 0 & 0 & 0 \\ 0 & 0 & -\sqrt{6}\Omega_- & 0 & 0 & 0 & 0 & 0 \end{bmatrix}.$$

The nonzero elements of the matrix L are

$$L(1,1)=1,\ L(2,2)=1,\ L(3,3)=1,$$

and the nonzero elements of the matrices $L_\mu(\mu=-1,0,+1)$ are $1/\sqrt{10}$ times:

$$L_{-1}(6,1)=1,\ L_{-1}(7,2)=\sqrt{3},\ L_{-1}(8,3)=\sqrt{6},$$

$$L_0(5,1)=\sqrt{3},\ L_0(6,2)=2,\ L_0(7,3)=\sqrt{3},$$

$$L_{+1}(4,1)=\sqrt{6},\ L_{+1}(5,2)=\sqrt{3},\ L_{+1}(6,3)=1.$$

We integrate this equation numerically using the fifth-order Runge-Kutta method.

[1] P. Marte, P. Zoller, and J. L. Hall, Phys. Rev. A **44**, R4118 (1991).
[2] J. Lawall and M. Prentiss, Phys. Rev. Lett. **72**, 993 (1994).
[3] L. S. Goldner, C. Gerz, R. J. C. Spreeuw, S. L. Rolston, C. I. Westbrook, W. D. Phillips, P. Marte, and P. Zoller, Phys. Rev. Lett. **72**, 997 (1994).
[4] H. Theuer and K. Bergmann, Eur. Phys. J. D **2**, 279 (1998).
[5] H. Theuer, R. G. Unanyan, C. Habscheid, K. Klein, and K. Bergmann, Opt. Express **4**, 77 (1999).
[6] N. V. Vitanov, M. Fleischhauer, B. W. Shore, and K. Bergmann, in *Advances in Atomic Molecular and Optical Physics*, 46, edited by B. Bederson, and H. Walther (Academic, New York, 2001), Vol. 46 pp. 55–190.
[7] R. Unanyan, M. Fleischhauer, B. W. Shore, and K. Bergmann, Opt. Commun. **155**, 144 (1998).
[8] R. G. Unanyan, B. W. Shore, and K. Bergmann, Phys. Rev. A **59**, 2910 (1999).
[9] F. Vewinger, M. Heinz, R. G. Fernandez, N. V. Vitanov, and K. Bergmann, Phys. Rev. Lett. **91**, 213001 (2003).
[10] B. W. Shore, K. Bergmann, J. Oreg, and S. Rosenwaks, Phys. Rev. A **44**, 7442 (1991).
[11] J. Oreg, K. Bergmann, B. W. Shore, and S. Rosenwaks, Phys. Rev. A **45**, 4888 (1992).
[12] L. M. Duan, J. I. Cirac, and P. Zoller, Science **292**, 1695

(2001).
[13] J. R. Morris and B. W. Shore, Phys. Rev. A **27**, 906 (1983).
[14] Z. Kis and S. Stenholm, J. Mod. Opt. **49**, 111 (2002).
[15] R. G. Unanyan and M. Fleischhauer, Phys. Rev. A **69**, 050302 (2004).
[16] B. W. Shore, *The Theory of Coherent Atomic Excitation* (Wiley, New York, 1990).
[17] N. V. Vitanov, Z. Kis, and B. W. Shore, Phys. Rev. A **68**, 063414 (2003).
[18] F. Wilczek and A. Zee, Phys. Rev. Lett. **52**, 2111 (1984).
[19] L. Faoro, J. Siewert, and R. Fazio, Phys. Rev. Lett. **90**, 028301 (2003).
[20] P. Meystre and M. Sargent III, *Elements of Quantum Optics*, (Springer-Verlag, New York, 1999).